Report of pilot study CCM.P-P1 for international comparison of absolute pressure measurements in gas from 3×10^{-9} Pa to 9×10^{-4} Pa

H. Yoshida[1], K. Arai[1], E. Komatsu[1], K. Fujii[1], T. Bock[2], K. Jousten[2]

---

[1] NMIJ/AIST: The National Metrology Institute of Japan / the National Institute of Advanced Science and Technology, Japan

[2] PTB: Physikalisch-Technische Bundesanstalt

Abstract

A bilateral comparison of absolute gas pressure measurements from 3×10^{-9} Pa to 9×10^{-4} Pa was performed between the National Metrology Institute of Japan (NMIJ) and Physikalisch-Technische Bundesanstalt (PTB). It is a pilot study CCM.P-P1 for the next international comparison in this pressure range to test the stability of ultrahigh vacuum gauges (UHV gauges) as transfer standards. Two spinning rotor gauges (SRGs), an axial-symmetric transmission gauge (ATG), and an extractor gauge (EXG) were used as transfer standards. The calibration ratio of one SRG was sufficiently stable, but the other was not. This result indicates that improvements in the transport mechanism for SRG are needed. The two ionization gauges ATG and EXG, on the other hand, were sufficiently stable. Provisional equivalence of the pressures realized by the primary standards at NMIJ and PTB was found.

1. Introduction

Key comparison CCM.P-K3 for absolute pressure measurements from 3×10^{-6} Pa to 9×10^{-4} Pa was performed from 1998 to 2002 to determine the degree of equivalence of national metrology institutes [1]. The follower of this comparison shall be extended down to 3×10^{-9} Pa as decided by the Low Pressure Working Group of the Consultative Committee for Mass and Related Quantities (CCM) in 2011. A pilot study CCM.P-P1 was performed in advance because there are two challenging issues in the CCM.P-K3 follower. The first is the transport and long-term stability of the ultrahigh vacuum gauges capable of measuring pressures as low as 3×10^{-9} Pa. UHV gauges are hot cathode ionization gauges with a structure that reduces disturbances from sources such as X-rays and electron-stimulated desorption (ESD) ions. The second is the stability of transfer gauges to repeated bake-outs, which are necessary to achieve these low pressures.

Initially, three types of UHV gauges, namely, axial-symmetric transmission gauges (ATG), extractor gauges (EXG), and a bent belt-beam gauge (3BG), were tested at the National Metrology Institute of Japan (NMIJ). Spinning rotor gauges (SRGs) were also tested to evaluate the stability against repeated baking-out. As in [1], the SRGs shall serve as transfer standards at 9×10^{-4} Pa to normalize the ion gauge results to correct for pressure-independent shifts in the ion gauge characteristics, since it can be expected that

the calibration ratio of the SRGs is more stable than that of the ion gauges. After the

tests at NMIJ, a draft protocol for the CCM.P-K3 follower was prepared based on the

previous CCM.P-K3. Following this protocol, a bilateral comparison for the absolute

gas pressure measurements from 3×10^{-9} Pa to 9×10^{-4} Pa was performed between NMIJ

and Physikalisch-Technische Bundesanstalt (PTB) to test the transport stability of the

transfer standards and the practicability of the protocol. This is the first international

comparison of the measurement of pressures down to 10^{-9} Pa.

2.   Stability test of transfer gauges in NMIJ
2.1   Stability test of three types of UHV gauges with the XHV standard
system

 Two ATGs, two EXGs, and one 3BG were tested in the extreme high vacuum (XHV)

standard system in NMIJ. The main specifications of these gauges are shown in Table 1.

The following five parameters were compared: background pressure readings, change in

pressure reading during gas introduction, effect of air exposure and baking-out, effect of

changing temperature, and long-term stability.

Table 1　　　　　　　Main specifications of the UHV gauges: ATG, EXG, and 3BG.

		ATG	EXG	3BG
Material	Filament	Y_2O_3-Ir	Y_2O_3-Ir	Y_2O_3-Ir
	Body	Stainless steel	Stainless steel	BeCu
Emission current [mA]		1.0	1.6	1.6
Grid voltage [V]		110	220	220
Filament voltage [V]		10	100	100
Nominal electron energy [eV]		100	120	120
Nominal sensitivity [Pa^{-1}]		0.023	0.066	0.05 - 0.07
Nominal measurement limit [Pa]		5×10^{-11}	10^{-10}	5×10^{-12}

2.1.1　Background pressure readings

Table 2 shows the typical background pressure readings of tested UHV gauges, which were measured at the same time in the XHV standard system in NMIJ after baking at 200 °C for 3 days. A thermally insulated box was used to contain the vacuum chamber including the UHV gauges during the baking to achieve a homogeneous temperature. The smallest pressure reading was indicated by ATG-1, which is a check standard of the XHV system. The values of ATG and 3BG were comparable. EXG showed larger values than the other gauges. The gauges connected with an all-metal valve (ATG-2 and EXG-2) showed larger values than those connected with an elbow.

5

The background pressure reading is mainly determined by two factors; one is the residual pressure in the vacuum chamber which is determined by both the ultimate pressure of the vacuum pump and the outgassing rate from the vacuum chamber. The other is the residual current of the UHV gauge which is caused by releasing secondary electrons from the ion collector, the X-ray effect, the effect of electron stimulated ions, the inverse X-ray effect, the ineluctable leak current and outgassing from the gauge itself, and so on. It is beyond the scope of this study to discuss which term is dominant or which gauge showed the value closest to the true one. Here, we conclude that these gauges showed background pressure readings comparable to the lowest calibration pressure of 3×10^{-9} Pa.

Table 2   Typical background pressure readings after baking-out at lower than 200 °C for 3 days for the XHV standard system at NMIJ.

	Connection	Type of controller	Background pressure reading [Pa]
ATG-1	Elbow (40CF)	ISX2	1.16×10^{-9}
ATG-2	All-metal valve (40CF)	ISX2	1.68×10^{-9}
EXG-1	Elbow (40CF)	IM520	2.61×10^{-9}
EXG-2	All-metal valve (40CF)	IM540	3.29×10^{-9}
3BG	Elbow (40CF)	IM540	1.84×10^{-9}

2.1.2 Change in pressure reading during gas introduction and nonlinearity

Figure 1 shows the change in pressure reading during gas introduction up to 2×10^{-9} Pa for (a) N_2 and (b) Ar. No significant difference in the fluctuation and drift of the pressure readings were observed, which agrees with previous reports [2-4]. The pressure readings for Ar were higher than those of N_2 because the ionization cross section of Ar is higher than that of N_2. The nonlinearities of the sensitivity for N_2 and Ar were less than $\pm$ 2 % which were comparable with earlier investigations [4]. Both N_2 and Ar are suitable as calibration gases for the international comparison.

(a)

(b)
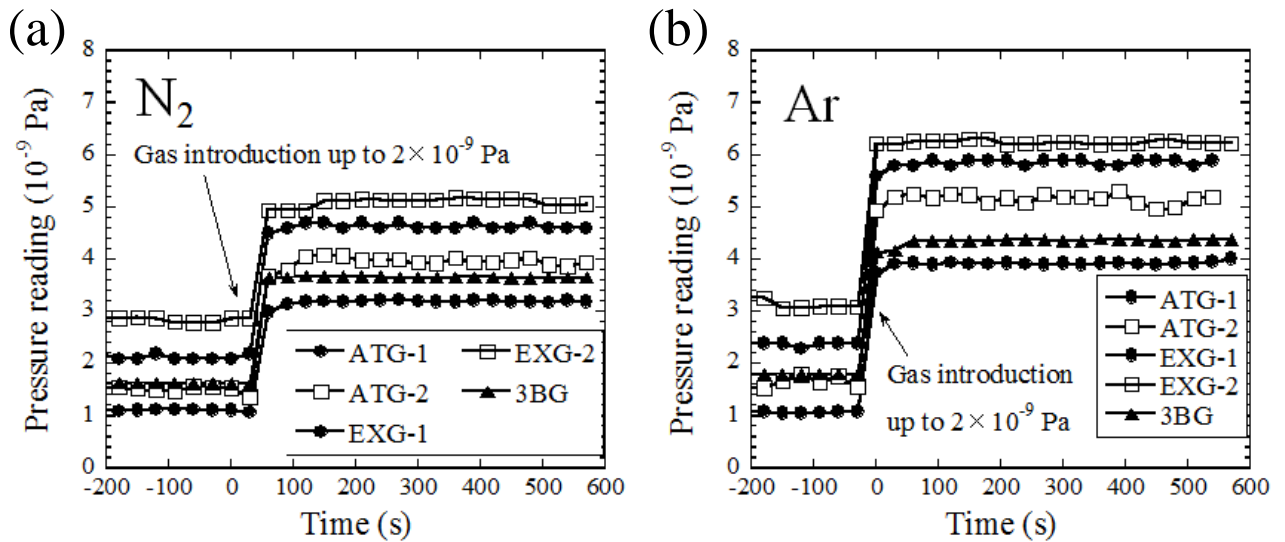
Figure 1   Change in pressure reading during gas introduction up to 2×10^{-9} Pa for (a) N_2 and (b) Ar.

2.1.3 Effect of air exposure and baking-out

To examine the effect of air exposure and baking-out, we applied the following procedure.

(i) Five gauges (ATG-1, ATG-2, EXG-1, EXG-2, and 3BG) were calibrated from 10^{-9} Pa to 10^{-6} Pa for N_2 after a first bake-out out (#1 in Fig.2).

(ii) Air exposure for ATG-2 and EXG-2 was performed by detaching the gauge heads from the all-metal valve after closing the valve. Typically, the relative humidity was 50% and the exposure time was several hours.

(iii) The whole calibration system, including the five gauges, was baked out at 200 °C for 3 days.

(iv) The gauges were recalibrated (#2).

(v) Air exposure for ATG-2 and EXG-2 was repeated.

(vi) The whole calibration system, including the gauges, was baked out at 200 °C for 3 days.

(vii) The gauges were recalibrated (#3).

(viii) ATG-2 and EXG-2 were recalibrated (#4) after turning ATG-1, EXG-1, and 3BG off.

Calibration results are summarized to calculate the inverse of the correction factor f_c^{-1} because f_c^{-1} is proportional to the sensitivity S as shown in ISO 27894,

$$f_c^{-1} = \frac{p_G - p_{G0}}{p - p_0} \propto S, \qquad - \ (1)$$

where p_G and p_{G0} are the gauge reading at the pressure p and at the residual pressure p_0, respectively. Figure 2 shows the change in mean f_c^{-1} from 10^{-9} Pa to 10^{-5} Pa for four calibration cycles. Because one calibration cycle includes three or four calibration runs, the total time for this test was about 2 months. The change in mean f_c^{-1}, which included both the instability of tested gauges and the reproducibility of XHV standard in NMIJ, was less than 3 %. The differences of both p_{G0} of tested gauges and p_0 among four calibration cycles, however, are not the origin of changing sensitivity because they are subtracted from p_G and p, respectively, as shown in eq. (1). No significant differences were observed among tested gauges from viewpoints of effect of air exposure and baking-out.
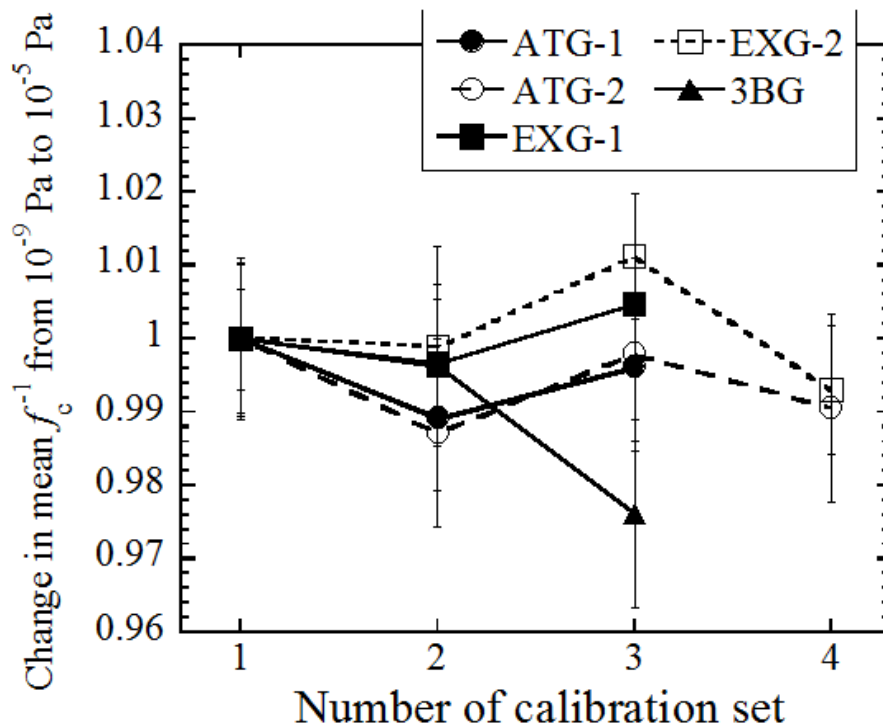
Figure 2   Change in the sensitivity S for four calibration cycles for two ATGs, two EXGs, and a 3BG. The mean sensitivities S from 10^{-9} Pa to 10^{-5} Pa for N_2 are plotted. The second and third cycle calibrations were carried out after air exposure for ATG-2 and EXG-2 and after baking-out. The fourth calibration cycle was carried out after turning ATG-1, EXG-1, and 3BG off.

2.1.4 Effect of changing the temperature

Increasing the temperature of the vacuum chamber for a constant injected molar flow rate has two effects. First, the background pressure reading is increased owing to increased outgassing from both the vacuum chamber and gauges. Second, the sensitivity of the UHV gauges is decreased because of the decreased gas density. These effects have been reported in UHV gauges [4,5] similar to typical hot cathode ionization gauges [6-8]. In addition, we changed the temperature of gauge controllers by placing them in a box with a temperature controller. The background pressure reading of ATG decreased from 7.0×10^{-9} Pa to 0.0×10^{-10} Pa by altering the controller temperature from 23 °C to 45 °C. However, a stable value of around 1.7×10^{-9} Pa was obtained after pushing the button to adjust the offset. On the other hand, the background pressure reading of EXG slightly increased from 3.0×10^{-9} Pa to 3.5×10^{-9} Pa by changing the controller temperature from 22 °C to 38 °C. The temperature coefficients of the pressure readings of ATG and EXG were roughly -0.4×10^{-9} Pa/K and 0.03×10^{-9} Pa/K, respectively. Particular care should be taken to stabilize the controller temperature of ATG during calibration. As mentioned before, the relevant calibration results were obtained by subtracting the background pressure readings just before gas introduction provided that the temperature was stable.

2.1.5　Long-term stability

Figure 3 shows the long-term stability of the five UHV gauges for 1200 days. The plotted points are the mean f_c^{-1} from 10^{-9} Pa to 10^{-5} Pa. Changes in sensitivity from 8 % to 13 % were observed for the test period, which are comparable with typical hot cathode ionization gauges [1-5,9-11]. No significant change was observed for the nonlinearity of sensitivity during the test period, which means that these long-term instabilities were caused by the shift of the sensitivity in the whole pressure range. The origin of these long-term shifts is still unclear although several possibilities are expected such as the changes in the hot filament, changing in the electron orbit, the contamination of ion collector, and so on. The long-term stability of SRG is much better than UHV gauges [12-22]. Therefore, employing SRG is necessary as additional transfer standard to normalize results of UHV gauges for a reliable international comparison.
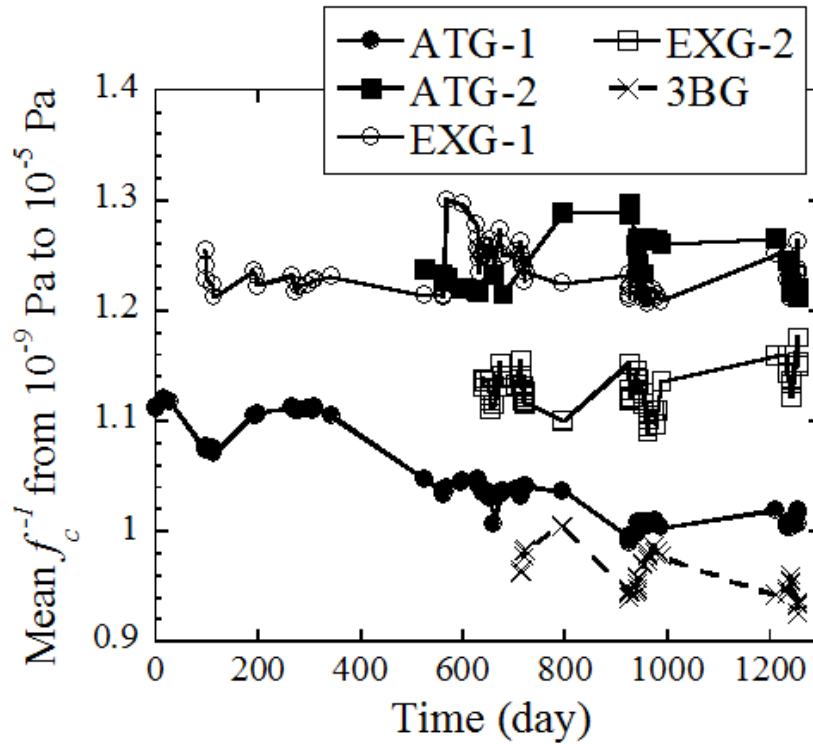
Figure 3　　　　Long-term stability of two ATGs, two EXGs, and a 3BG for 1200 days. The plotted points are mean sensitivity S from 10^{-9} Pa to 10^{-6} Pa for N_2.

2.2　　SRG stability to repeated baking-out

The stability of the effective accommodation coefficient, σ_{eff}, of SRG-1 and SRG-2 against repeated baking-out was tested by using a direct comparison system with an SRG reference standard (SRG-R) at NMIJ. Another SRG (SRG-C) was simultaneously tested as a check standard on the system. The rotors of SRG-1, SRG-R and SRG-C were made of stainless steel, but that of SRG-2 was Invar. Four SRGs were attached to the system at the same time and compared. When the thimble flanges of both SRG-1 and SRG-2 were baked out or exposed to air for tests, both SRG-R and SRG-C were in

vacuum without bake-out to keep their σ_{eff} stable. The test results are summarized in Fig. 4.

The change in σ_{eff} for SRG-1, SRG-2, and SRG-C was less than 0.02 % during the first nine measurements. Air exposure when a spring was added to fix the rotor during shipping made the σ_{eff} smaller by 0.09 % for SRG-1 and 0.36 % for SRG-2, respectively (point (i), Fig. 4). Subsequently, the σ_{eff} for SRG-1 and SRG-2 became stable to within 0.2 %. Significant increases were observed after the first bake-out of 2.7 % for SRG-1 and 0.98 % for SRG-2 (point (ii), Fig. 4). However, no significant difference was observed after the second and third bake-outs. A previous study reported similar behavior for σ_{eff} [23]. Air exposure after baking-out decreased σ_{eff} to 0.31 % for SRG-1 and 0.11 % for SRG-2, respectively (point (iii), Fig. 4). Re-baking of both gauges recovered the σ_{eff} values to within 0.01% of their original values before air exposure (point (iv), Fig. 4). Following this, similar changes were observed after air exposure and baking-out. This behavior has not been reported previously [12]. Detaching and attaching the suspension head from the thimble did not greatly affect σ_{eff}; the peak-to-peak value of the stability of σ_{eff} after the first bake-out is within 0.44 % for SRG-1 and 0.17 % for SRG-2, respectively.
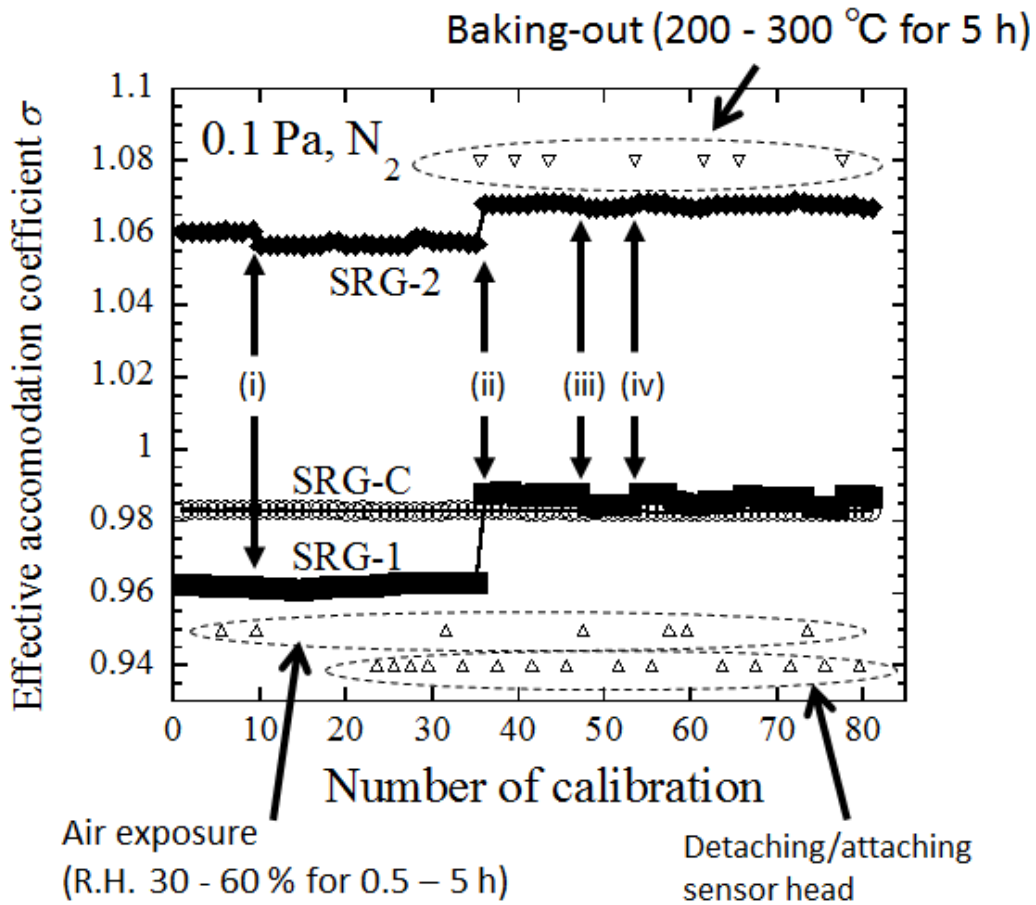
Figure 4   Results of the stability of SRG to repeated baking-out. Symbols ∇, $\triangle$, and $\blacktriangle$ show the time when the thimble was baked-out at 200 - 300 $^{\circ}$C for 5 h, the inside of thimble ant rotor was exposure to air with the relative humidity (R.H.) of 30 –60 % for 0.5 – 5 h, and the suspension head of SRG was removed and attached. Point (i) indicates when a spring to fix the rotor is added to the thimble of SRG. Similarly, points (ii), (iii), and (iv) indicate when SRG-1 and SRG-2 were baked out for the first time, when they were exposed to air, and when they were re-baked, respectively.

3. Bilateral comparison between NMIJ and PTB from 3×10^{-9} Pa to 9×10^{-4} Pa.

3.1 Protocol

The main points of the protocol are summarized in Table 3. Transfer standards are calibrated at twelve target pressure (P_T) from 3×10^{-9} Pa to 9×10^{-4} Pa. The requirement to the background pressure readings before the calibrations was less than twice as large as the lowest target pressure. In addition, the pressure generated by each vacuum standard was required to be within 10 % of the target pressure. Each sequence is repeated a minimum of two times on different days (minimum three calibration runs). NMIJ used two standard systems to cover the whole calibration range, while PTB used one standard system. N_2 gas with a purity higher than 99.999 % was used as a calibration gas because it is the typical calibration gas for ionization gauges.

ATG-2, EXG-2, SRG-1, and SRG-2 were used as transfer standards. ATG-2 and EXG-2 were selected because these are conventional gauges, although the stability of 3BG was comparable. Degassing and changing the parameters of ATG-2 and EXG-2 were prohibited during measurements. SRGs were used to normalize the calibration results of ATG-2 and EXG-2 at a calibration pressure of 9×10^{-4} Pa. Both the gauge head and the controller of ATG-2 and EXG-2 were shipped, but the sensor heads (thimble including rotor and suspension head) without their controllers were shipped for the two SRGs. The type of the controller was SRG-2CE for NMIJ and SRG-2 for PTB,

respectively.

In addition, the time schedule, how to pack and ship transfer standards, how to install and remove transfer gauges, the calibration procedures, and items to be reported were described in the protocol.

Table 3   Main protocol points for this pilot study.

Items	Requirements	Comments
Target pressure	3×10^{-9} Pa, 9×10^{-9} Pa, 3×10^{-8} Pa, 9×10^{-8} Pa, 3×10^{-7} Pa, 9×10^{-7} Pa, 3×10^{-6} Pa, 9×10^{-6} Pa, 3×10^{-5} Pa, 9×10^{-5} Pa, 3×10^{-4} Pa, and 9×10^{-4} Pa	Calibration pressure shall be set within ±10 % of the target pressure
Gas	N_2	Purity > 99.999 %
Transfer standards	ATG (AxTRAN, ULVAC, Inc.) EXG (IONIVAC (IE514), Oerlikon Leybold Vacuum) Two SRGs (MKS Instruments, Inc.)	ATG, EXG for whole the target pressure range. Two SRGs for 9×10^{-4} Pa only. SRG controllers are not shipped
Bake-out	Limited to less than 200 °C	Owing to the heatproof temperature of the ATG
Background pressure reading	Less than twice as large as the lowest target pressure	
Standard system	Use of more than two systems is allowed	NMIJ uses two systems
Room temperature	23 ± 1 °C	
Chamber temperature	Not specified, but must be measured	

3.2   Primary vacuum standards

NMIJ used two calibration systems: a ultrahigh vacuum (UHV) standard system with a continuous expansion system (CES, also called the orifice flow method) from 3×10^{-6} Pa to 9×10^{-4} Pa [24,25] by using a constant pressure flow meter [26]; and an XHV standard system with a two-stage flow dividing system from 3×10^{-9} Pa to 3×10^{-6} Pa [4].

PTB used a continuous expansion system from 3×10^{-9} Pa to 9×10^{-4} Pa [27]. The system has a UHV chamber and an XHV chamber. The UHV chamber was used in this test. The flow meter [28] applying the constant pressure and constant conductance method were used to determine the flow rate from 9×10^{-4} Pa to 3×10^{-7} Pa and from 9×10^{-8} Pa to 3×10^{-9} Pa, respectively.

3.3   Measurements

Table 4 shows the chronology and number of measurements. There were some problems during the measurements. Both SRG-1 and SRG-2 did not work after shipping from NMIJ to PTB, and from PTB to NMIJ because of the deformation of the spring used to fix the rotor. Furthermore, there was a leak at the thimble flanges of both SRGs in PTB. Therefore, we had to repair the SRGs before the measurements. Then the rotors and the inside of the thimble flanges of the SRGs were exposed to air for about one day.

Other problems with the computer control of transfer gauges also occurred. However, all measurements were completed successfully.

Table 4   Chronology and number of measurements at a specific target point pressure.

Participants		Start date	End date	Number of calibration runs, N_{run}	Number points per run, N_{point}	Total number of points, N_{ijm}
NMIJ /AIST	XHV	May 30, 2013	31 May 2013	4	9	36
	CES1	Jun 17, 2013	19 June 2013	3	6	18
PTB		Oct 24, 2013	31 October 2013	6 (SRGs) 2-10 (IGs)	4 (SRGs) 5 (IGs)	24 (SRGs) 10-50 (IGs)
NMIJ /AIST	CES2	Jan 8, 2014	15 January 2014	3	6	18

The typical values of the background pressure readings of UHV gauges and the residual drag (RD) of SRGs during calibration are listed in Table 5. Transfer standards were baked-out at a temperature somewhat lower than 200 ^{o}C for several days before calibrations at NMIJ-XHV and PTB, but were not baked-out at NMIJ-CES. Another B-A type hot cathode ionization gauge (BAG-C) and two other SRGs (SRG-C1 and SRG-C2), which are always attached to NMIJ-CES as check standards, were simultaneously calibrated with the transfer standards to confirm the stability of

NMIJ-CES between two cycles.

Table 5   Typical values of background pressure readings of the UHV gauges
               and RD of the SRGs during calibrations.

		SRG-1 [1/s]	SRG-2 [1/s]	ATG-2 [Pa]	EXG-2 [Pa]
NMIJ-XHV	p_{BG}	-	-	1.88×10^{-9}	3.20×10^{-9}
NMIJ-CES1	RD or p_{G0}	7.95×10^{-7}	6.11×10^{-8}	2.33×10^{-7}	2.23×10^{-7}
PTB	RD or p_{G0}	9.50×10^{-7}	6.77×10^{-8}	3.77×10^{-9}	4.61×10^{-9}
NMIJ-CES2	RD or p_{G0}	4.50×10^{-6}	5.94×10^{-8}	1.04×10^{-7}	1.40×10^{-7}

4.   Indices for abbreviated terms

The meanings of the indices for the abbreviated terms used in this report are

summarized in Table 6. A calibration cycle is the whole calibration, from receiving the

transfer standards to returning them. Therefore, the number of calibration cycles, m, for

NMIJ-CES has values of 1 and 2, whereas those of NMIJ-XHV and PTB are 1. One

calibration cycle includes several calibration runs, and one calibration run includes

many calibration points. The total number of calibration points per calibration cycle,

N_{ijm}, equals the product of the number of calibration runs, N_{run}, and the number of

calibration points, N_{point}. Table 4 shows N_{run}, N_{point}, and N_{ijm} for each cycle at a specific

target point pressure. k is a transfer gauge reading at a calibration point.

Table 6   Meanings of the indices for the abbreviated terms.

Index		Meaning
i		Transfer standard gauges
	1	SRG-1
	2	SRG-2
	3	ATG
	4	EXG
j		Institute and calibration system
	1	NMIJ-CES
	2	NMIJ-XHV
	3	PTB
m		Number of calibration cycles
k		Individual gauge reading at a calibration point

5. Results and discussion

5.1 Analysis of the reported data at 9×10^{-4} Pa based on SRGs

5.1.1 Calibration ratio at 9×10^{-4} Pa

The calibration ratio of a_{ijm} (commonly referred to as effective accommodation coefficient, σ_{eff}) is calculated from equation (2),

$$a_{ijm} = \frac{1}{N_{ijm}} \sum_{k=1}^{N_{ijm}} a_{ijmk} = \frac{1}{N_{ijm}} \sum_{k=1}^{N_{ijm}} \frac{p_{ijmk}}{P_{ijmk}}, \qquad - (2)$$

where p_{ijmk} is the pressure reading of SRG i, calibration system j, cycle m, and reading k, P_{ijmk} is the pressure generated by the vacuum standards, and $N_{1jm} = N_{2jm}$.

Figure 5 shows the calibration ratios, a_{ijm}, obtained for the two transfer SRGs and two SRGs for check standards of NMIJ-CES. The values of a_{ijm} for SRG-2, SRG-C1, and SRG-C2 were relatively stable, while a_{1jm} for SRG-1 increased in chronological order. Table 7 shows the shift in the calibration ratios of four SRGs for the two calibration cycles of NMIJ-CES. The results of the two check standards indicate the stability of NMIJ-CES between two cycles being less than 0.12 %, which is smaller than the long term shift of a_{ijm} for two transfer SRGs. The shift in a_{2jm} before and after shipping was about 0.28 %, which is comparable to or slightly larger than the results of the pretest in NMIJ (see Fig. 4). Changes in a_{1jm} of more than 3 % are much larger than the results of

the pretest. The problems during measurements must have affected these results. However, the magnitude of the change in the calibration ratios is within the range of those observed during previous international comparisons from 0.00 % to 4.2 % [18-27]. In this report, data analysis using only SRG-2 was carried out because the change in a_{1jm} for SRG-1 was larger than the change in the sensitivity of the UHV gauges, as discussed below.
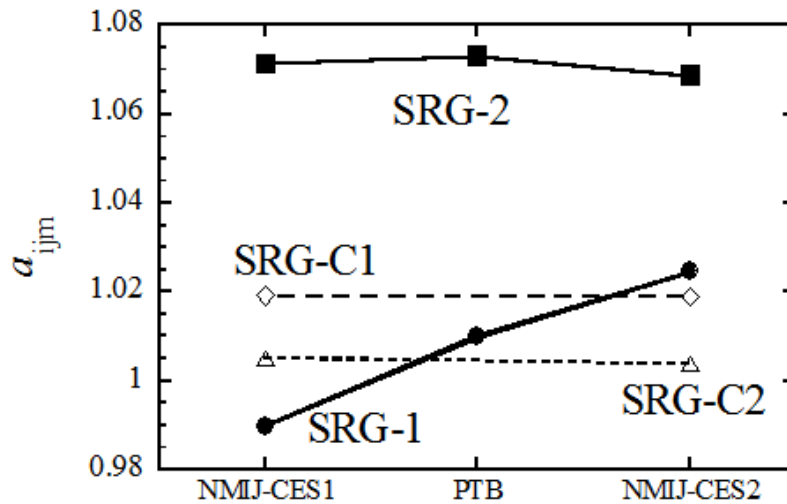
Figure 5   Calibration ratios, a_{ijm}, for the two transfer SRGs (SRG-1 and SRG-2) measured at NMIJ-CES and PTB. Calibration ratios for the two check standards of NMIJ-CES (SRG-C1 and SRG-C2) are also shown.

Table 7 Shift in the calibration ratios of the two SRGs for the two calibration cycles of NMIJ-CES.

	NMIJ-CES1	NMIJ-CES2	$a_{i12} - a_{i11}$
SRG-1	0.9900	1.0247	0.0347
SRG-2	1.0715	1.0686	-0.0028
SRG-C1	1.0192	1.0191	0.0001
SRG-C2	1.0051	1.0039	0.0012

23

5.1.2 Determination of mean gauge pressure reading, p_j, at 9×10^{-4} Pa

A predicted gauge pressure reading for SRG-2 ($p_{2\text{jm}}$), which is the value when calibration system j at calibration cycle m is set to a target pressure ($P_\text{T} = 9 \times 10^{-4}$ Pa), is calculated from equation (3),

$$p_{2jm} = a_{2jm} \cdot P_T. \qquad - \ (3)$$

For the continuous expansion system in NMIJ (NMIJ-CES), the mean gauge pressure reading, p_j, was calculated as the arithmetic mean of the two cycle values,

$$p_j = \frac{p_{2j1} + p_{2j2}}{2}, \qquad - \ (4)$$

where $p_{2\text{j}1}$ and $p_{2\text{j}1}$ are the predicted pressure readings of the first and second cycles, respectively, of NMIJ-CES. The mean gauge pressure reading of PTB equals the predicted pressure readings, as PTB had only one calibration cycle.

5.1.3 Estimation of the standard uncertainty of mean gauge pressure reading at 9×10^{-4} Pa

The standard uncertainty of the mean gauge pressure reading, $u(p_\text{j})$, of NMIJ and PTB is estimated by equations (5) and (6), respectively,

$$u^2(p_j) = \frac{1}{2^2} \sum_{m=1}^{2} u^2(p_{2jm}) \qquad (j = 1;\ NMIJ - CES), \qquad - (5)$$

$$u(p_j) = u(p_{2jm}) \qquad (j = 3;\ PTB). \qquad - (6)$$

Model equation (7) is used to estimate the standard uncertainty of the predicted pressure

reading of SRG-2, $u(p_{2jm})$, from equation (3).

$$p_{2jm} = a_{2jm} \cdot P_T + \delta p_{std} + \delta p_{LTS}. \qquad - (7)$$

where δp_{std} and δp_{LTS} are the biases of the standard pressure arising from each vacuum

standard and from the long-term shift of a_{2jm}, respectively. Although these values are

assumed to be zero because they are unknown, they are important for calculating the

uncertainty by (8),

$$u(p_{2jm}) = \sqrt{\left(P_T \cdot u_A(a_{2jm})\right)^2 + u^2(\delta p_{std}) + u^2(\delta p_{LTS})} . \qquad - (8)$$

The uncertainty of the target pressure $u(P_T) = 0$ because P_T is a nominal value. The type

A uncertainty of a_{2jm}, $u_A(a_{2jm})$, is estimated from the standard deviation of the mean of

each run, $s_r(a_{ijm})$, of the repeated measurements of a_{2jm} with the number of runs, N_{run}, for cycle m. $u(\delta p_{std})$ and $u(\delta p_{LTS})$ are the standard uncertainties arising from the standard pressure and that owing to long-term shift of a_{2jm}, respectively. The value of $u(\delta p_{std})$ is reported by participants. The value of $u(\delta p_{LTS})$ is calculated from the difference of calibration results before and after shipping at NMIJ-CES by equation (9),

$$\frac{u(\delta p_{LTS})}{p_{2jm}} = \frac{u_{LTS}(a_{2jm})}{a_{2jm}} = \frac{1}{2} \cdot \frac{|a_{2j1} - a_{2j2}|}{a_{2j1}}. \qquad - \quad (9)$$

Although the type B uncertainty of both temperature $u(T)$ and the residual drag $u(RD)$ have previously been included to estimate $u(p_{2jm})$ [1, 18-21], these terms are not included in equation (8) to avoid double counting of the uncertainty with $u_A(a_{2jm})$ (see Appendix 1). The contribution of the display resolution of the controller is discussed in Appendix 2. Table 8 lists the calibration ratio (a_{ijm}), predicted pressure reading (p_{ijm}), standard uncertainty contributions to $u_c(p_{ijm})$, and the combined standard uncertainty ($u_c(p_{ijm})$).

5.2   Analysis of the reported data from 3×10^{-9} Pa to 9×10^{-4} Pa based on the UHV gauges

5.2.1   Calibration ratio from 3×10^{-9} Pa to 9×10^{-4} Pa

For ATG ($i = 3$) and EXG ($i = 4$) for calibration system j, cycle m, and reading k,

pressure reading p_{ijmk} is calculated from the following equation,

$$p_{ijmk} = p_{Gijmk} - p_{G0ijmk}. \qquad\qquad -\ (10)$$

Here, p_{Gijmk} and p_{G0ijmk} are the gauge reading during gas introduction and the background pressure readings, respectively. The calibration ratio, a_{ijm} (commonly referred to as the inverse of the correction factor f_c^{-1}), is calculated for the two transfer UHV gauges of ATG-2, EXG-2 and the NMIJ-CES check standard of BAG-C, similar to the calculation for SRG by using equation (2). Figure 6 shows a_{ijm} of ATG-2, EXG-2 and BAG-C. Changes in a_{ijm} of both ATG-2 and EXG-2 were comparable to or smaller than the results of the pretest (Fig. 2 and 3). The difference in the results of the XHV standard in NMIJ (NMIJ-XHV) and NMIJ-CES for EXG may look large, but it is within the range of the change observed in the long-term stability test. The non-linearity of BAG-C between 9×10^{-5} Pa and 3×10^{-4} Pa was caused by the automatic change in the emission current due to the controller. Table 9 shows the shift in the calibration ratios of ATG-2, EXG-2 and BAG-C for the two calibration cycles of NMIJ-CES. The result of BAG-C supports the conclusion mentioned in the section 5.1.1 that the stability of NMIJ-CES between two cycles is less than 0.12 % at least. The shift of a_{ijm} before

27

Table 8   Calibration ratio, a_{ijm}, predicted pressure reading, p_{ijm}, standard uncertainty contributions to $u_c(p_{ijm})$, and the combined standard uncertainty, $u_c(p_{ijm})$ at 9×10^{-4} Pa.

	a_{2jm}	p_{2jm} [Pa]	Standard uncertainty [Pa]			$u(p_{2jm})$ [Pa]
			$u(a_{2jm}) \cdot P_T$	$u(\delta p_{std})$	$u(\delta p_{LTS})$	
NMIJ-CES1	1.0715	9.643×10^{-4}	2.64×10^{-7}	1.10×10^{-5}	1.27×10^{-6}	1.11×10^{-5}
PTB	1.0730	9.657×10^{-4}	5.61×10^{-7}	2.30×10^{-6}	1.27×10^{-6}	2.69×10^{-6}
NMIJ-CES2	1.0686	9.618×10^{-4}	7.21×10^{-7}	1.10×10^{-5}	1.27×10^{-6}	1.11×10^{-5}

Table 9   Shift in the calibration ratios of ATG-2 and EXG-2 for the two calibration cycles of NMIJ-CES.

	P_T [Pa]	NMIJ-CES1	NMIJ-CES2	$a_{i12} - a_{i11}$
ATG-2	3×10^{-6}	1.222	1.228	0.006
	9×10^{-6}	1.198	1.204	0.006
	3×10^{-5}	1.201	1.213	0.012
	9×10^{-5}	1.199	1.214	0.016
	3×10^{-4}	1.201	1.224	0.023
	9×10^{-4}	1.179	1.213	0.034
EXG-2	3×10^{-6}	1.068	1.080	0.012
	9×10^{-6}	1.066	1.075	0.010
	3×10^{-5}	1.068	1.080	0.012
	9×10^{-5}	1.064	1.082	0.018
	3×10^{-4}	1.064	1.080	0.016
	9×10^{-4}	1.068	1.083	0.015
BAG-C	3×10^{-6}	0.993	0.987	0.005
	9×10^{-6}	0.996	0.992	0.004
	3×10^{-5}	0.995	0.989	0.006
	9×10^{-5}	0.992	0.989	0.003
	3×10^{-4}	0.944	0.938	0.006
	9×10^{-4}	0.952	0.952	0.000

and after shipping was from -0.1 % to 3.4 % for ATG-2 and from 1.0 % to 1.8 % for EXG-2. The change in EXG in this study was much smaller than that observed in previous work (~12 %) [15].

5.2.2 Ion gauge calibration ratio from 3×10^{-9} Pa to 3×10^{-4} Pa

The ion gauge calibration ratio, $K_{jm}(P_T)$, is defined by equation (11) to normalize the calibration ratios of ATG-2 and EXG-2 with that of SRG-2. The normalization assumes that the generated pressure of the vacuum standard at 9×10^{-4} Pa was the same whether it was being measured with UHV gauges or an SRG.

$$K_{ijm}(P_T) = \frac{a_{ijm}(P_T)}{a_{ijm}(9 \times 10^{-4} \, Pa)} \cdot \frac{p_j(9 \times 10^{-4} \, Pa)}{p_R}, \qquad - \quad (11)$$

where $p_j(9 \times 10^{-4}$ Pa) is determined by SRG-2, and p_R is the reference pressure, which is numerically equal to 9×10^{-4} Pa. In addition, the calibration results of NMIJ-XHV are normalized by those of NMIJ-CES at 3×10^{-6} Pa.

$$K_{i2m}(P_T) = \frac{a_{i2m}(P_T)}{a_{i2m}(3 \times 10^{-6} \, Pa)} \cdot K_{i1m}(3 \times 10^{-6} \, Pa), \qquad - \quad (12)$$
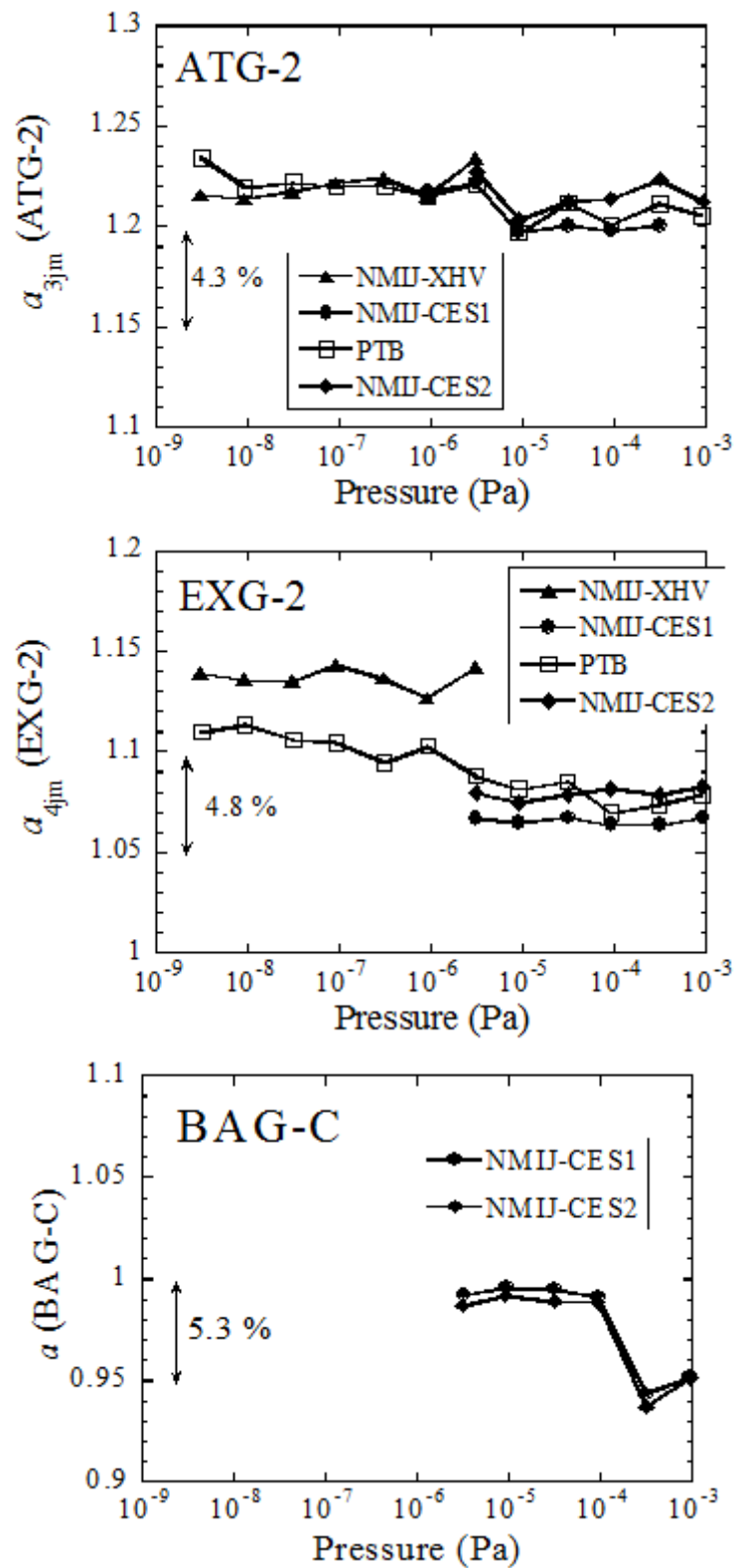
Figure 6   Calibration ratios, a_{ijm}, of ATG-2 and EXG-2 measured at NMIJ-CES. NMIJ-XHV and PTB. Calibration ratio for the check standard of NMIJ-CES (BAG-C) is also shown.
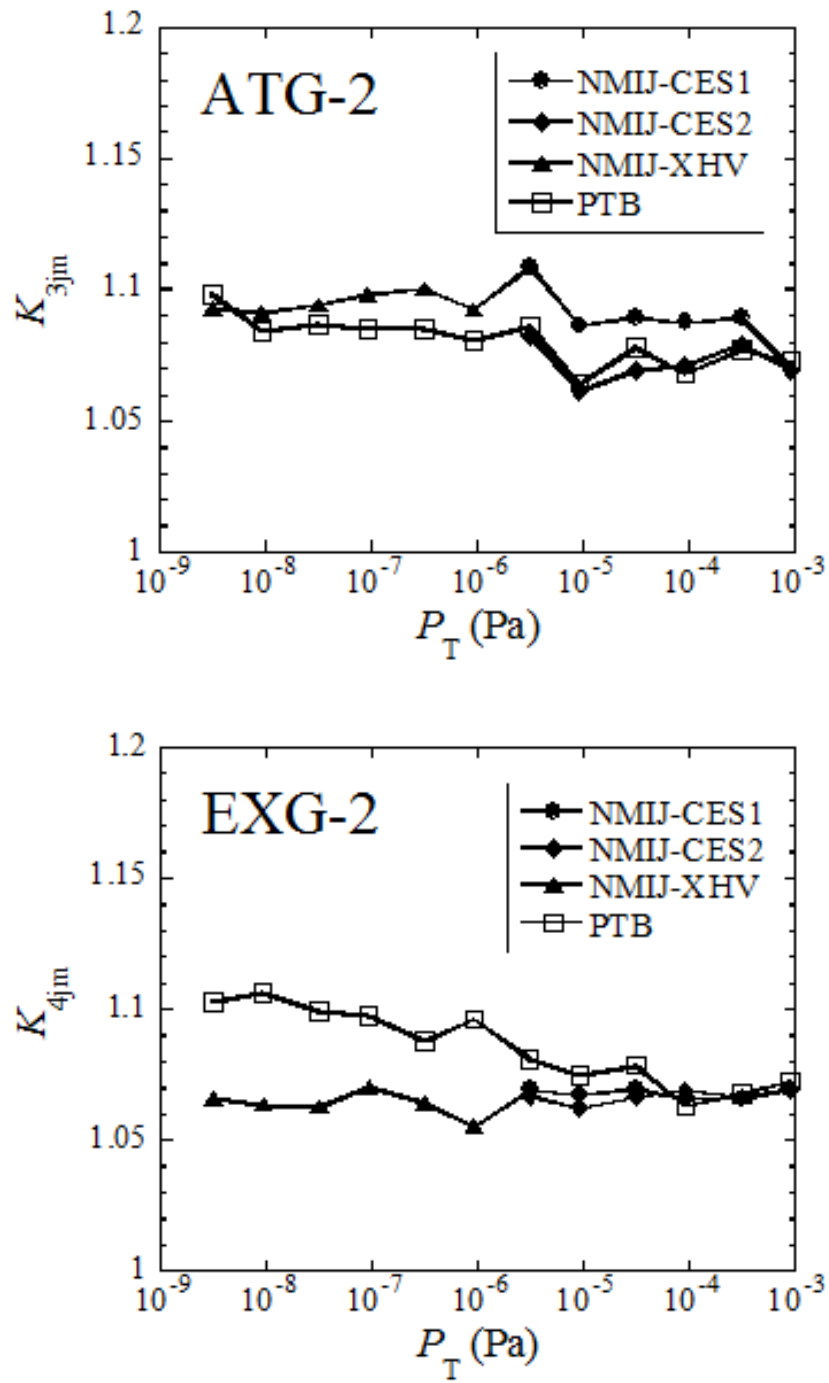
Figure 7   Ion gauge calibration ratio, $K_{jm}(P_T)$, obtained by participants as a function of the target pressure, P_T.

where $K_{\text{i1m}}(3 \times 10^{-6}$ Pa) is the ion gauge calibration ratio of the first cycle calibration of

NMIJ-CES at the target pressure of 3×10^{-6} Pa. This normalization is justified, since

NMIJ-XHV is traceable to NMIJ-CES and not an independent standard [4]. Figure 7

shows $K_{\text{jm}}(P_{\text{T}})$ obtained by participants as a function of the target pressure, P_{T}.

5.2.3 Determination of mean gauge pressure reading from 3×10^{-9} Pa to 3×10^{-4} Pa

The predicted gauge pressure reading, p_{ijm}, for ATG-2 and EXG-2 is calculated from

equation (13),

$$p_{ijm} = K_{ijm} \cdot P_T . \qquad - \ (13)$$

A single gauge pressure reading is useful for comparing the pressures of the calibration

systems. A mean cycle gauge pressure reading, p_{jm}, was calculated as the simple

arithmetic mean of the predicted gauge readings of ATG-2 and EXG-2

$$p_{jm} = \frac{p_{3jm} + p_{4jm}}{2} . \qquad - \ (14)$$

32

where p_{3jm} and p_{4jm} are the predicted pressure readings of ATG-2 and EXG-2, respectively. The mean gauge pressure reading, p_j, of NMIJ-CES was calculated as the arithmetic mean of the two cycle values, similar to equation (4). p_j of NMIJ-XHV was normalized by p_j of NMIJ-CES. These calculations allow us to present a single value from NMIJ. The mean gauge pressure reading of PTB equals its predicted pressure readings.

5.2.4   Estimation of the standard uncertainty from 3 × 10^{-9} Pa to 3 × 10^{-4} Pa based on two UHV gauges

The type A uncertainty of the ion gauge calibration ratio, $u_A(K_{ijm})$ is determined from equation (15), for NMIJ-CES and PTB,

$$
\frac{u_A\left(K_{ijm}(P_T)\right)}{K_{ijm}(P_T)}
$$

$$
= \sqrt{\left(\frac{u_A\left(a_{ijm}(P_T)\right)}{a_{ijm}(P_T)}\right)^2 + \left(\frac{u_A\left(a_{ijm}(9 \times 10^{-4}\ \text{Pa})\right)}{a_{ijm}(9 \times 10^{-4}\ \text{Pa})}\right)^2 + \left(\frac{u_A\left(a_{2jm}(9 \times 10^{-4}\ \text{Pa})\right)}{a_{2jm}(9 \times 10^{-4}\ \text{Pa})}\right)^2}
$$

$$
(i = 3, 4). \quad - \quad (15)
$$

Here, the $u_A(a_{ijm}(P_T))$ and the $u_A(a_{ijm}(9 \times 10^{-4}\ \text{Pa}))$ are the type A uncertainties of a_{ijm} at P_T and 9×10^{-4} Pa, respectively, which are equal to the standard deviation of the mean of

each run $s_r(a_{ijm})$ of the repeated measurements of a_{ijm} (i=3, 4) at the pressure. The

$u_A(a_{2jm}(9 \times 10^{-4}$ Pa)) is the type A uncertainty of a_{2jm} at 9×10^{-4} Pa measured by SRG-2.

The type A uncertainty, $u_A(K_{ijm})$, for NMIJ-XHV is estimated from equation (16)

$$\frac{u_A\left(K_{i2m}(P_T)\right)}{K_{i2m}(P_T)}$$
$$= \sqrt{\left(\frac{u_A\left(a_{i2m}(P_T)\right)}{a_{i2m}(P_T)}\right)^2 + \left(\frac{u_A\left(a_{i2m}(3 \times 10^{-6} \, Pa)\right)}{a_{i2m}(3 \times 10^{-6} \, Pa)}\right)^2 + \left(\frac{u_A\left(K_{i1m}(3 \times 10^{-6} \, Pa)\right)}{K_{i1m}(3 \times 10^{-6} \, Pa)}\right)^2}$$

$$(i = 3, 4). \quad - \quad (16)$$

Here, the $u_A(a_{i2m}(P_T))$ and the $u_A(a_{i2m}(3 \times 10^{-6}$ Pa)) are the type A uncertainties of a_{ijm}

at P_T and 3×10^{-6} Pa, respectively, measured by NMIJ-XHV. The $u_A(K_{i1m}(3 \times 10^{-6}$ Pa))

are the type A uncertainty of K_{i1m} at 3×10^{-6} Pa measured by NMIJ-CES, which was

calculated by the eq.(15).

The standard uncertainty of the predicted gauge pressure reading, $u(p_{ijm})$, from 3×10^{-9}

Pa to 3×10^{-4} Pa is calculated from equation (17) similar to equation (8) for SRG,

$$u(p_{ijm}) = \sqrt{\left(P_T \cdot u_A\left(K_{ijm}\right)\right)^2 + u^2(\delta p_{std}) + u^2(\delta p_{LTS})} \quad (i = 3, 4) \, .$$
$$- \quad (17)$$

Here, the $u_A(K_{ijm})$ is calculated by the eq.(15) or the eq.(16). The standard uncertainties

of the standard pressure of each vacuum standard, $u(\delta p_{std})$, is reported by participants.

The standard uncertainty originated from the long-term shift of K_{ijm}, $u(\delta p_{LTS})$, is

estimated from the mean of the one half of the difference of K_{ijm} before and after

shipping at NMIJ-CES to prevent the value of $u(\delta p_{LTS})$ from being accidentally small.

This estimation assumes that the long-term shift of the sensitivity of UHV gauges has

negligible pressure dependence. The mean of the one half of the difference of K_{ijm} is

0.010 for ATG and 0.002 for EXG, which corresponds to the relative standard

uncertainty originated from the long-term shift, $u(\delta p_{LTS})/p_{ijm}$, for the whole pressure

range. Table 10 lists standard uncertainty contributions to $u_c(p_{ijm})$, and the combined

standard uncertainty $u_c(p_{ijm})$ for NMIJ-CES, NMIJ-XHV, and PTB.

 The standard uncertainty of the mean cycle gauge pressure reading, $u(p_{jm})$, was

calculated by the equation (18)

$$u(p_{jm}) = \sqrt{\frac{u^2(p_{3jm}) + u^2(p_{4jm})}{2}}, \qquad - \ (18)$$

where $u(p_{3jm})$ and $u(p_{4jm})$ are the standard uncertainties of the predicted pressure

readings of ATG-2 and EXG-2, respectively. The standard uncertainty of the mean

gauge pressure reading, $u(p_j)$, of NMIJ-CES was calculated by the equation (19),

$$u(p_1) = \sqrt{\frac{u^2(p_{11}) + u^2(p_{12})}{2}}. \qquad - (19)$$

where $u(p_{11})$ and $u(p_{12})$ are the standard uncertainties of the mean cycle gauge pressure

reading of 1st cycle and 2nd cycle, respectively. The $u(p_j)$ of NMIJ-XHV and PTB equals

their $u(p_{jm})$. Calculation results are summarized in Table 11.

5.3   Comparison results

Table 11 summarizes the mean gauge pressure reading, p_j, and the standard uncertainty,

$u(p_j)$, for NMIJ and PTB. The pair-wise difference d, its expanded uncertainty ($k = 2$),

$U(d)$, and the degree of equivalence, En, which are defined by equations (20)-(22),

respectively, are also shown in Table 11.

$$d = p_{PTB} - p_{NMIJ} \qquad - (20)$$

$$U(d) = 2 \cdot u(d) = 2 \cdot \sqrt{u^2(p_{PTB}) + u^2(p_{NMIJ})} \qquad - (21)$$

$$E_n = \frac{|d|}{U(d)} \qquad - (22)$$

The pair-wise difference shown in Fig. 8 was less than 3 % from 3×10^{-9} Pa to 9×10^{-4}

Pa. The values of E_n were less than unity over the whole pressure range, which means

that the calibration results of PTB and NMIJ were equivalent.
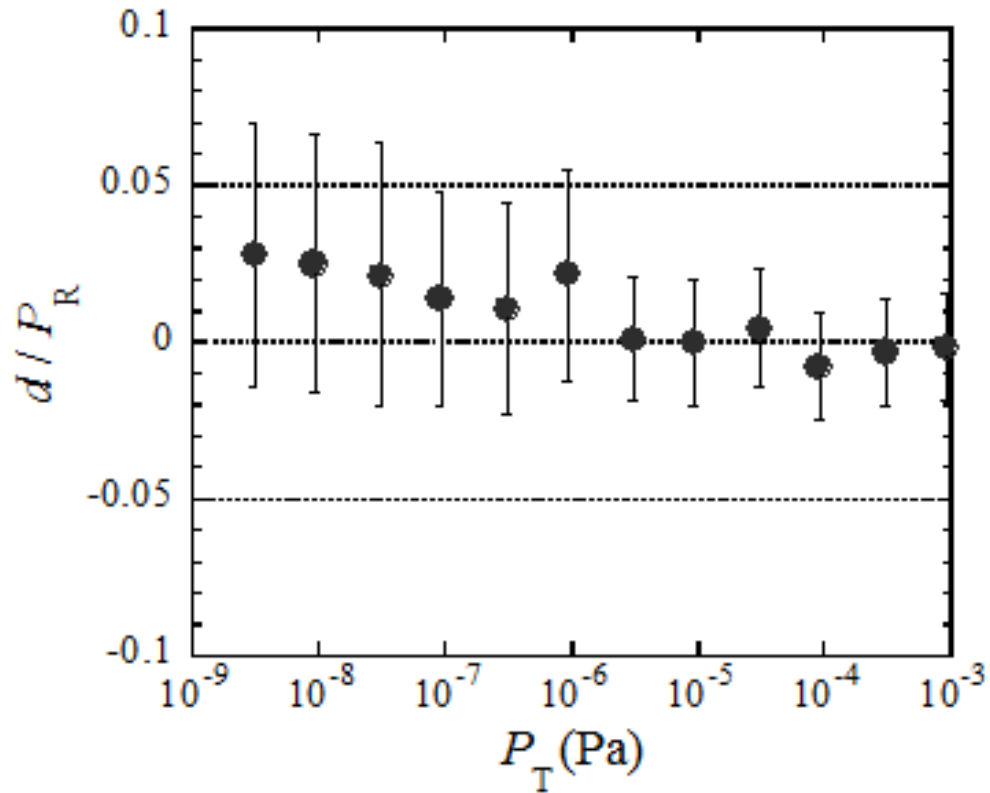
Figure 8   Pair-wise difference of the mean gauge pressure reading, p_j, between NMIJ and PTB.

Table 10   Standard uncertainty contributions to $u_c(p_{ijm})$, and the combined standard uncertainty, $u_c(p_{ijm})$, for NMIJ-CES, NMIJ-XHV, and PTB from 3×10^{-9} Pa to at 3×10^{-4} Pa.

(a) NMIJ-CES1

P_T [Pa]	$u(p_{std})$ [Pa]	Standard uncertainty of p_{3jm} by ATG-2 [Pa]			Standard uncertainty of p_{4jm} by EXG-2 [Pa]		
		$u_A(K_3) P_T$	$u(\delta p_{LTS})$	$u_c(p_{3jm})$	$u_A(K_4) P_T$	$u(\delta p_{LTS})$	$u_c(p_{4jm})$
3×10^{-6}	4.00×10^{-8}	1.57×10^{-9}	3.41×10^{-8}	5.26×10^{-8}	8.76×10^{-9}	6.49×10^{-9}	4.15×10^{-8}
9×10^{-6}	1.10×10^{-7}	9.80×10^{-9}	1.00×10^{-7}	1.49×10^{-7}	9.90×10^{-9}	1.95×10^{-8}	1.12×10^{-7}
3×10^{-5}	3.64×10^{-7}	1.93×10^{-8}	3.35×10^{-7}	4.95×10^{-7}	5.61×10^{-8}	6.50×10^{-8}	3.74×10^{-7}
9×10^{-5}	1.09×10^{-6}	4.37×10^{-8}	1.00×10^{-6}	1.48×10^{-6}	1.16×10^{-7}	1.94×10^{-7}	1.11×10^{-6}
3×10^{-4}	3.63×10^{-6}	2.46×10^{-7}	3.35×10^{-6}	4.95×10^{-6}	4.18×10^{-7}	6.47×10^{-7}	3.71×10^{-6}

(b) NMIJ-CES2

P_T [Pa]	$u(p_{std})$ [Pa]	Standard uncertainty of p_{3jm} by ATG-2 [Pa]			Standard uncertainty of p_{4jm} by EXG-2 [Pa]		
		$u_A(K_3) P_T$	$u(\delta p_{LTS})$	$u_c(p_{3jm})$	$u_A(K_4) P_T$	$u(\delta p_{LTS})$	$u_c(p_{4jm})$
3×10^{-6}	3.99×10^{-8}	1.03×10^{-8}	3.32×10^{-8}	5.29×10^{-8}	7.32×10^{-9}	$6.46 \times 10\text{-}9$	4.11×10^{-8}
9×10^{-6}	1.10×10^{-7}	2.94×10^{-8}	9.77×10^{-8}	1.50×10^{-7}	1.24×10^{-8}	1.93×10^{-8}	1.12×10^{-7}
3×10^{-5}	3.65×10^{-7}	8.96×10^{-8}	3.28×10^{-7}	4.98×10^{-7}	4.00×10^{-8}	6.46×10^{-8}	3.72×10^{-7}
9×10^{-5}	1.09×10^{-6}	3.12×10^{-7}	9.85×10^{-7}	1.50×10^{-6}	6.47×10^{-7}	1.94×10^{-7}	1.28×10^{-6}
3×10^{-4}	3.65×10^{-6}	9.37×10^{-7}	3.31×10^{-6}	5.02×10^{-6}	5.01×10^{-7}	6.46×10^{-7}	3.74×10^{-6}

(c) NMIJ-XHV

P_T /Pa	$u(p_{std})$ / Pa	Standard uncertainty of p_{3jm} by ATG-2 [Pa]			Standard uncertainty of p_{4jm} by EXG-2 [Pa]		
		$u_A(K_3)\,P_T$	$u(\delta p_{LTS})$	$u_c(p_{3jm})$	$u_A(K_4)\,P_T$	$u(\delta p_{LTS})$	$u_c(p_{4jm})$
3×10^{-9}	6.64×10^{-11}	1.16×10^{-11}	3.36×10^{-11}	7.54×10^{-11}	1.67×10^{-11}	6.48×10^{-12}	6.88×10^{-11}
9×10^{-9}	1.99×10^{-10}	3.30×10^{-11}	1.01×10^{-10}	2.26×10^{-10}	4.51×10^{-11}	1.94×10^{-11}	2.05×10^{-10}
3×10^{-8}	6.66×10^{-10}	1.27×10^{-10}	3.36×10^{-10}	7.57×10^{-10}	1.63×10^{-10}	6.46×10^{-11}	6.89×10^{-10}
9×10^{-8}	1.99×10^{-9}	3.99×10^{-10}	1.01×10^{-9}	2.27×10^{-9}	4.66×10^{-10}	1.95×10^{-10}	2.06×10^{-9}
3×10^{-7}	6.67×10^{-9}	1.32×10^{-9}	3.38×10^{-9}	7.59×10^{-9}	1.58×10^{-9}	6.47×10^{-10}	6.88×10^{-9}
9×10^{-7}	1.98×10^{-8}	3.86×10^{-9}	1.01×10^{-8}	2.25×10^{-8}	4.87×10^{-9}	1.92×10^{-9}	2.05×10^{-8}

(d) PTB

P_T [Pa]	$u(p_{std})$ [Pa]	Standard uncertainty of p_{3jm} by ATG-2 [Pa]			Standard uncertainty of p_{4jm} by EXG-2 [Pa]		
		$u_A(K_3)\,P_T$	$u(\delta p_{LTS})$	$u_c(p_{3jm})$	$u_A(K_4)\,P_T$	$u(\delta p_{LTS})$	$u_c(p_{4jm})$
3×10^{-9}	5.72×10^{-11}	2.82×10^{-11}	3.37×10^{-11}	7.21×10^{-11}	1.17×10^{-11}	6.69×10^{-12}	5.87×10^{-11}
9×10^{-9}	1.67×10^{-10}	4.35×10^{-11}	9.99×10^{-11}	1.99×10^{-10}	2.83×10^{-11}	2.01×10^{-11}	1.71×10^{-10}
3×10^{-8}	5.80×10^{-10}	4.06×10^{-11}	3.34×10^{-10}	6.71×10^{-10}	4.82×10^{-11}	6.67×10^{-11}	5.87×10^{-10}
9×10^{-8}	5.02×10^{-10}	1.11×10^{-10}	1.00×10^{-9}	1.12×10^{-9}	2.19×10^{-10}	2.00×10^{-10}	5.84×10^{-10}
3×10^{-7}	1.51×10^{-9}	5.06×10^{-10}	3.33×10^{-9}	3.69×10^{-9}	9.43×10^{-10}	6.60×10^{-10}	1.90×10^{-9}
9×10^{-7}	4.63×10^{-9}	2.92×10^{-9}	9.96×10^{-9}	1.14×10^{-8}	4.32×10^{-9}	1.99×10^{-9}	6.65×10^{-9}
3×10^{-6}	1.54×10^{-8}	6.92×10^{-9}	3.33×10^{-8}	3.74×10^{-8}	6.98×10^{-9}	6.56×10^{-9}	1.81×10^{-8}
9×10^{-6}	4.55×10^{-8}	2.58×10^{-8}	9.81×10^{-8}	1.11×10^{-7}	3.39×10^{-8}	1.96×10^{-8}	6.00×10^{-8}
3×10^{-5}	1.52×10^{-7}	9.50×10^{-8}	3.31×10^{-7}	3.76×10^{-7}	1.03×10^{-7}	6.54×10^{-8}	1.95×10^{-7}
9×10^{-5}	2.29×10^{-7}	3.02×10^{-7}	9.84×10^{-7}	1.05×10^{-6}	1.57×10^{-7}	1.93×10^{-7}	3.39×10^{-7}
3×10^{-4}	7.36×10^{-7}	5.67×10^{-7}	3.31×10^{-6}	3.44×10^{-6}	4.75×10^{-7}	6.48×10^{-7}	1.09×10^{-6}

Table 11　　　　　　The mean gauge pressure reading, p_j, and the standard uncertainty, $u(p_j)$, for NMIJ and PTB from 3×10^{-9} Pa to at 9×10^{-4} Pa..

P_T [Pa]	p_j [Pa]		d [Pa]	$u(p_j)$ [Pa]		$U(d)$ [Pa]	E_n
	NMIJ	PTB		NMIJ	PTB		
3×10^{-9}	3.219×10^{-9}	3.302×10^{-9}	8.37×10^{-11}	5.1×10^{-11}	4.6×10^{-11}	1.4×10^{-10}	0.61
9×10^{-9}	9.636×10^{-9}	9.863×10^{-9}	2.27×10^{-10}	1.5×10^{-10}	1.3×10^{-10}	4.0×10^{-10}	0.56
3×10^{-8}	3.215×10^{-8}	3.280×10^{-8}	6.50×10^{-10}	5.1×10^{-10}	4.5×10^{-10}	1.4×10^{-9}	0.48
9×10^{-8}	9.698×10^{-8}	9.826×10^{-8}	1.29×10^{-9}	1.5×10^{-9}	6.3×10^{-10}	3.3×10^{-9}	0.39
3×10^{-7}	3.227×10^{-7}	3.261×10^{-7}	3.34×10^{-9}	5.1×10^{-9}	2.1×10^{-9}	1.1×10^{-8}	0.30
9×10^{-7}	9.605×10^{-7}	9.801×10^{-7}	1.96×10^{-8}	1.5×10^{-8}	6.6×10^{-9}	3.3×10^{-8}	0.59
3×10^{-6}	3.247×10^{-6}	3.252×10^{-6}	4.68×10^{-9}	2.5×10^{-8}	2.1×10^{-8}	6.6×10^{-8}	0.07
9×10^{-6}	9.628×10^{-6}	9.630×10^{-6}	1.31×10^{-9}	7.2×10^{-8}	6.3×10^{-8}	1.9×10^{-7}	0.01
3×10^{-5}	3.222×10^{-5}	3.236×10^{-5}	1.41×10^{-7}	2.2×10^{-7}	2.1×10^{-7}	6.1×10^{-7}	0.23
9×10^{-5}	9.663×10^{-5}	9.595×10^{-5}	-6.73×10^{-7}	6.3×10^{-7}	5.5×10^{-7}	1.7×10^{-6}	0.40
3×10^{-4}	3.227×10^{-4}	3.219×10^{-4}	-8.29×10^{-7}	2.0×10^{-6}	1.8×10^{-6}	5.3×10^{-6}	0.16
9×10^{-4}	9.630×10^{-4}	9.657×10^{-4}	2.67×10^{-6}	7.8×10^{-6}	2.7×10^{-6}	1.7×10^{-5}	0.16

6. Conclusion

In this pilot study CCM.P-P1, we validated the transfer standards and the protocol for absolute gas pressure measurements from 3×10^{-9} Pa to 9×10^{-4} Pa. Transfer standards are generally considered to be sufficiently stable when the uncertainty arising from the primary standard, $u(p_{std})$, becomes the dominant factor in the total standard uncertainty, $u(p_{j})$. Although SRG-2 was sufficiently stable despite problems during the measurements in this study, the changes in SRG-1 were unacceptable. Improving the transfer SRG is necessary for more reliable international comparisons.

For the UHV gauges, the uncertainty caused by transport and long-term shift was comparable to or smaller than $u(p_{std})$ of NMIJ (Table 10 (a), (b), and (c)). $u(\delta p_{LTS})$ of EXG-2 was also comparable to or smaller than $u(p_{std})$ of PTB, while $u(\delta p_{LTS})$ of ATG-2 was several times larger than $u(p_{std})$ of PTB. ATG, however, has the advantage that the background pressure reading is lower than that of EXG. The result of the long-term stability test (Fig. 3) shows that the long-term shift of EXG is not always smaller than that of ATG. If a long-term shift of several percent is acceptable, international comparisons down to 10^{-9} Pa can be achieved by using our protocol. However, further improvements and discussions are necessary for more precise comparisons.

Appendix 1   Contribution of type B uncertainty of temperature and RD

In this appendix, we explain why the type B uncertainty of temperature and RD was not included in equation (8) as previously reported in refs. [29] and [30].

The pressure reading of SRG, p_{read}, is calculated from following equation

$$p_{read} = \sqrt{\frac{8RT}{\pi M}} \cdot \frac{\pi d\rho}{20} \cdot (DCR - RD). \qquad - (A1)$$

Here, R and M are the gas constant and molar mass, respectively. d and ρ are the diameter and the density of the rotor, respectively.

One calibration cycle includes several calibration runs, N_{run}. One calibration run includes many calibration points, N_{point}. For the xth run, the average of the SRG readings, $\overline{p_x}$, and the dispersion, $V(p_{xy})$, are shown in equations (A2) and (A3), respectively,

$$\overline{p_x} = \frac{1}{N_{point}} \sum_{y=1}^{N_{point}} p_{xy}, \qquad - (A2)$$

$$V(p_{xy}) = \frac{\sum_{y=1}^{N_{point}} (p_{xy} - \overline{p_x})^2}{N_{point} - 1}, \qquad - (A3)$$

where p_{xy} is the reading of SRG at the yth point of run x. For each cycle, the average of the readings, $\bar{\bar{p}}$, and its dispersion, $V(\overline{p_x})$, are shown by equation (A4) and (A5), respectively.

$$\bar{\bar{p}} = \frac{1}{N_{run}} \sum_{x=1}^{N_{run}} \overline{p_x}, \qquad -(A4)$$

$$V(\overline{p_x}) = \frac{\sum_{x=1}^{N_{run}}(\overline{p_x} - \bar{\bar{p}})^2}{N_{run} - 1}, \qquad -(A5)$$

Here, the data structure of this measurement is considered. The result of each calibration cycle consists of several calibration runs (Fig. A1(a)). Therefore, the SRG reading at the yth point of run x, p_{xy}, is shown by equation (A6)

$$p_{xy} = \mu + \alpha_x + e_{xy}, \qquad -(A6)$$

where μ is the population mean of overall measurement, α_x is the difference between μ and the population mean of xth run μ_x, and e_{xy} is the data scattering during each run (Fig. A1(b)). The drift of the temperature and RD between runs becomes the origin of α_x. On the other hand, e_{xy} arises from the stability of the pressure in the vacuum chamber and noise during xth run.
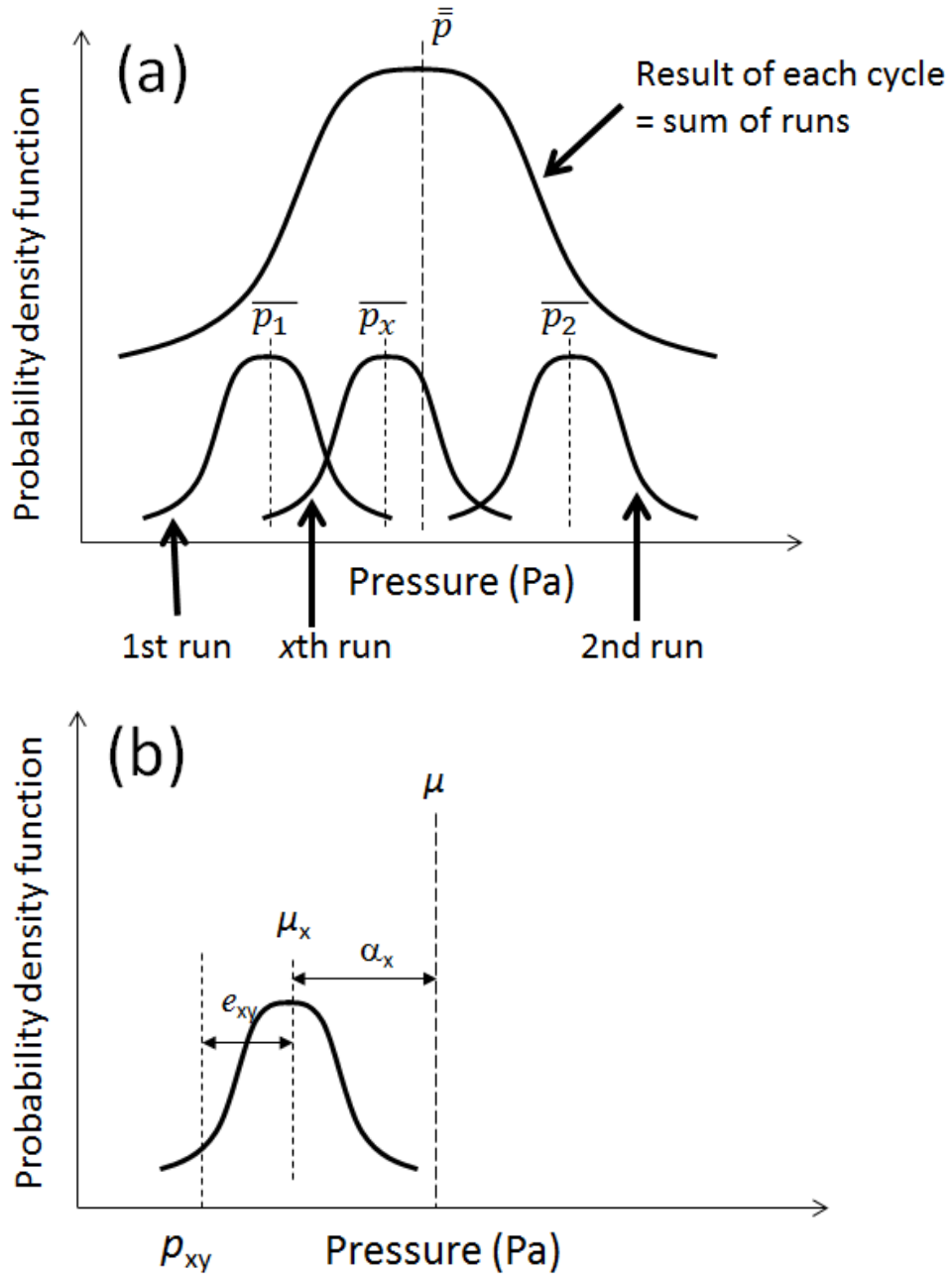
Figure A1   Data structure of measurements. (a) Each calibration cycle consists of several calibration runs, where $\bar{\bar{p}}$ and $\overline{p_x}$ are overall average pressure reading for each cycle, and the average for the xth run. (b) The data structure of p_{xy}. μ is the population mean of overall measurement, α_x is the difference between μ and the population mean of xth run μ_x, and e_{xy} is the data scattering during each run.

From equations (A2), (A4), and (A6), $\bar{\bar{p}}$ and $\bar{p}$ can be expressed as

$$\bar{\bar{p}} = \frac{1}{N_{run} \cdot N_{point}} \sum_{x=1}^{N_{run}} \sum_{y=1}^{N_{point}} (\mu + \alpha_x + e_{xy})$$

$$= \mu + \frac{1}{N_{run}} \sum_{x=1}^{N_{run}} \alpha_x + \frac{1}{N_{run} \cdot N_{point}} \sum_{x=1}^{N_{run}} \sum_{y=1}^{N_{point}} e_{xy}$$

$$= \mu + \overline{\alpha_x} + \overline{\overline{e_{xy}}} \qquad - (A7)$$

$$\overline{p_x} = \frac{1}{N_{point}} \sum_{y=1}^{N_{point}} (\mu + \alpha_x + e_{xy})$$

$$= \mu + \alpha_x + \frac{1}{N_{point}} \sum_{y=1}^{N_{point}} e_{xy}$$

$$= \mu + \alpha_x + \overline{e_{xy}}. \qquad - (A8)$$

By substituting equations (A7) and (A8) into equation (A5),

$$V(\overline{p_x}) = \frac{1}{N_{run} - 1} \sum_{x=1}^{N_{run}} \left(\alpha_x + \overline{e_{xy}} - \overline{\alpha_x} - \overline{\overline{e_{xy}}}\right)^2$$

$$= \frac{1}{N_{run} - 1} \sum_{x=1}^{N_{run}} \left((\alpha_x - \overline{\alpha_x}) + \left(\overline{e_{xy}} - \overline{\overline{e_{xy}}}\right)\right)^2$$

$$= \frac{\sum_{x=1}^{N_{run}}(\alpha_x - \overline{\alpha_x})^2}{N_{run} - 1} + \frac{\sum_{x=1}^{N_{run}}\left(\overline{e_{xy}} - \overline{\overline{e_{xy}}}\right)^2}{N_{run} - 1} + 2\frac{\sum_{x=1}^{N_{run}}(\alpha_x - \overline{\alpha_x}) \cdot \left(\overline{e_{xy}} - \overline{\overline{e_{xy}}}\right)}{N_{run} - 1}$$

If there is no correlation between α_x and e_{xy}, then $(\alpha_x - \overline{\alpha_x}) \cdot \left(\overline{e_{xy}} - \overline{\overline{e_{xy}}}\right) = 0$. Thus, equation (A9) is obtained as

$$V(\overline{p_x}) = \frac{\sum_{x=1}^{N_{run}}(\alpha_x - \overline{\alpha_x})^2}{N_{run} - 1} + \frac{\sum_{x=1}^{N_{run}}\left(\overline{e_{xy}} - \overline{\overline{e_{xy}}}\right)^2}{N_{run} - 1}. \qquad - (A9)$$

Here, the first term on right-hand side corresponds to the uncertainty arising from the drift of temperature and RD between runs. The second term is the uncertainty arising from data scattering of the SRG readings during each run.

In equation (8), the type A uncertainty, $u_A(a_{2jm})$, represents the standard deviation of the average values of each run, $s_r(\overline{p_x})$, which is numerically equal to the square root of $V(\overline{p_x})$. Because equation (A9) indicates that $V(\overline{p_x})$ includes the uncertainty arising from the drift of both temperature and RD, it is unnecessary to add the type B uncertainty arising from the drift of both temperature and RD to equation (8).

If necessary, type B uncertainties arising from both the calibration of the thermometer and temperature distribution of the calibration chamber should be added to equation (8). However, the effect of these uncertainties is sufficiently small and is estimated to be less than 0.05 %, even if these uncertainties are 0.3 K because the effect on the pressure reading of SRG is through the square root of temperature, as shown in equation (A1).

Appendix 2 Contribution of the type B uncertainty of the display resolution

The contribution of the standard uncertainty originated from the display resolution of

the controllers, $u_{\mathrm{res}}(p_{\mathrm{G}})$ where p_{G} is the gauge reading, to the total uncertainty is

discussed by using the same model of Appendix 1. The contribution of $u_{\mathrm{res}}(p_{\mathrm{G}})$ depends

on the correlation of the magnitude between $u_{\mathrm{res}}(p_{\mathrm{G}})$ and the standard deviation of the

mean of the gauge reading obtained at the xth run, $s(p_{\mathrm{xy}}) = \sqrt{V(p_{xy})}$, or the standard

deviation of the mean of the average value $\overline{p_x}$ obtained throughout the cycle,

$s_{\mathrm{r}}(\overline{p_x}) = \sqrt{V(\overline{p_x})}$. Figure A2 shows the typical three cases of the magnitude correlation of

$u_{\mathrm{res}}(p_{\mathrm{G}})$, $s(p_{\mathrm{xy}})$, and $s_{\mathrm{r}}(\overline{p_x})$.

The case (a) is when $u_{\mathrm{res}}(p_{\mathrm{G}})$ is much smaller than $s(p_{\mathrm{xy}})$, as shown in Fig. A2(a). Since

the contribution of $u_{\mathrm{res}}(p_{\mathrm{G}})$ is negligible, no need to add the term of the $u_{\mathrm{res}}(p_{\mathrm{G}})$ to the

equations of (8) and (17).

The case (b) is when $u_{\mathrm{res}}(p_{\mathrm{G}})$ is much larger than $s_{\mathrm{r}}(p_{\mathrm{xy}})$ but smaller than $s_{\mathrm{r}}(\overline{p_x})$. In this

case, $s(p_{\mathrm{xy}})$ equals to zero because the gauge reading p_{G} shows the same value during

the run. The $u_{\mathrm{res}}(p_{\mathrm{G}})$ becomes the Type B uncertainty of the gauge reading during each

run. However, there is no difference between the cases of (a) and (b) from the viewpoint

of the data structure, although the shapes of the probability distribution of each run are

different. In the case (a), the $s(p_{\mathrm{xy}})$ is included in the $V(\overline{p_x})$ as the second term of

(a) $s(p_{xy}) \gg u_{res}(p_G)$
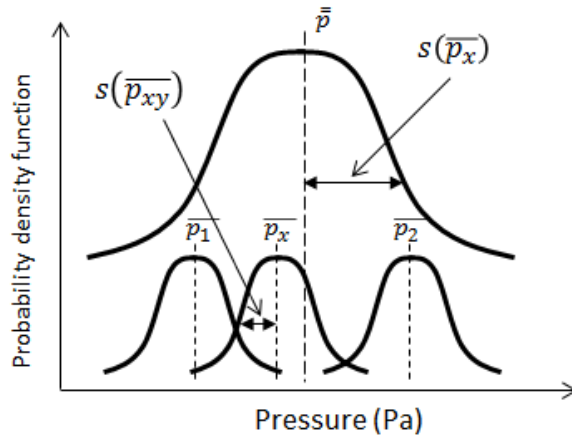
(b) $s(p_{xy}) \ll u_{res}(p_G) \ll s(\overline{p_x})$
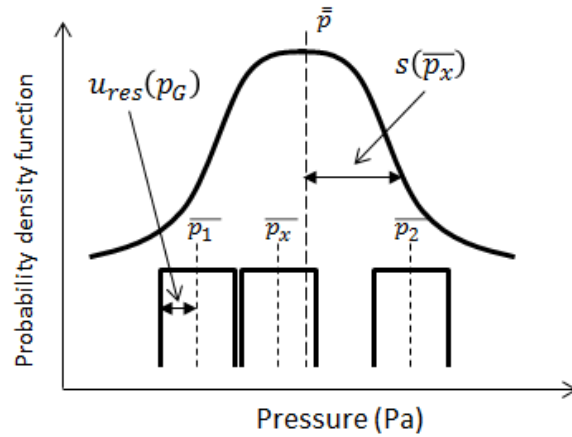
(c) $u_{res}(p_G) \gg s(\overline{p_x})$
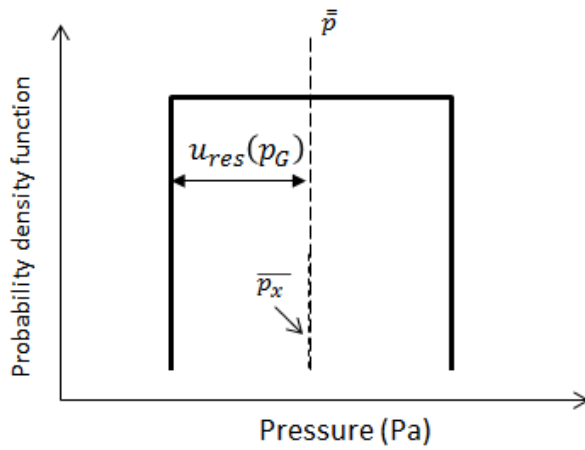
Figure A2   Typical three cases of the magnitude correlation of the standard uncertainty originated from the display resolution of the controllers, $u_{res}(p_G)$, the standard deviation of mean of the gauge reading at the xth run, $s_r(p_{xy})$, and that of the average value $\overline{p_x}$ throughout the cycle, $s_r(\overline{p_x})$.

right-hand side of the eq. (A9). In the case (b), the $u_{\text{res}}(p_G)$ is similarly included in the

$V(\overline{p_x})$ as the second term of right-hand side of the eq. (A9) instead of the $s(p_{xy})$.

Therefore, no need to add the term of the $u_{\text{res}}(p_G)$ in the equations of (8) and (17) in the

case (b), too.

The case (c) is when $u_{\text{res}}(p_G)$ is much larger than $s_r(\overline{p_x})$, as shown in Fig. A2(c). Since

the gauge reading p_G shows the same value throughout the cycle, $s_r(p_{xy}) = s_r(\overline{p_x}) = 0$. In

this case, the $u_{\text{res}}(p_G)$ must be added in the equations of (8) and (17).

Figure A3 shows the comparison of the magnitudes of $s_r(\overline{p_x})$ and $u_{\text{res}}(p_G)$. The ratio of

$s_r(\overline{p_x})/\overline{p_x}$ corresponds to the $u_A(a_{\text{ijm}})/a_{\text{ijm}}$ for SRGs and the $u_A(K_i)/K_i$ ($i=3, 4$) for UHV

gauges. These values are calculated from data in Table 8 and Table 10. To simplify the

Fig. 3, these results are shown without distinguishing where the data was obtained.

The display resolution, p_{res}, is 0.0001×10^{-z} Pa for SRG and 0.01×10^{-z} Pa for ATG

when the target pressure P_T is (3 or 9)$\times 10^{-z}$ Pa ($z = 4 \sim 9$). That of EXG at P_T is $0.01 \times$

10^{-z} Pa when the display of the controller is visually read and 0.0001×10^{-z} Pa when the

computer communication by RS-232C is used. The ratio of $u_{\text{res}}(p_G)/\overline{p_x}$ is roughly

estimated by the equation (A10) because the values of a_{ijm} for SRG-2 and K_{ijm} ($i=3,4$)

for UHV gauges are close to unity.

$$\frac{u_{res}(p_G)}{\overline{p_x}} \approx \frac{p_{res}}{2\sqrt{3}} \cdot \frac{1}{P_T}. \qquad -(A10)$$

Here, the uniform probability distribution is assumed.

The result of Fig. A3 indicates that the magnitudes of $s_r(\overline{p_x})$ is larger than that of $u_{res}(p_G)$. Therefore, it is unnecessary to add the term of the $u_{res}(p_G)$ in the equations of (8) and (17) in this case.
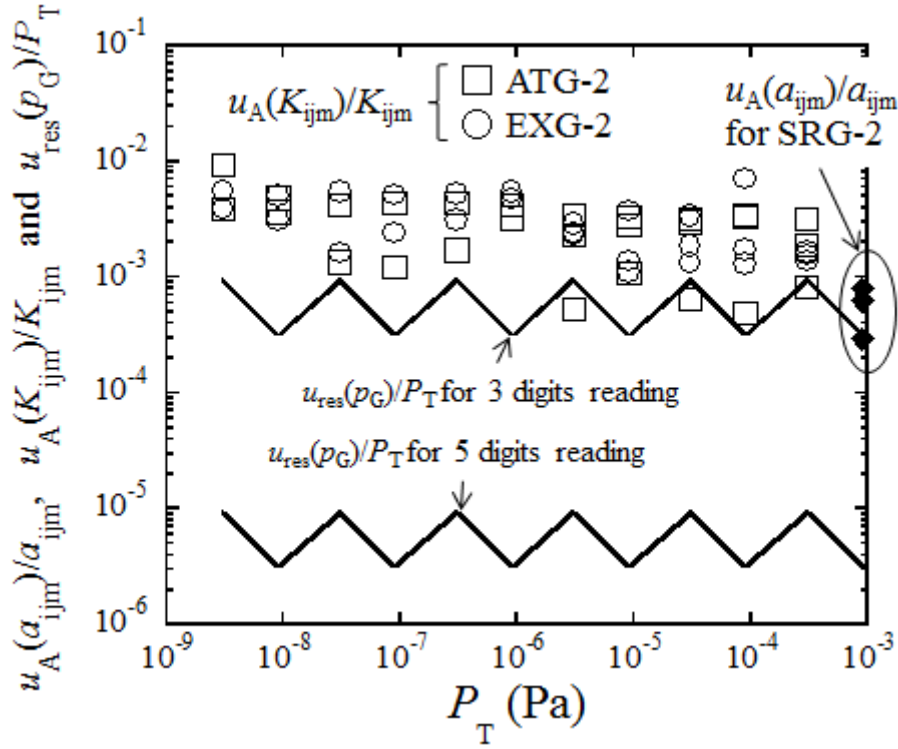
Figure A3   Comparison of the magnitudes of the $u_A(a_{ijm})/a_{ijm}$ for SRGs, the $u_A(K_i)/K_i$ (i=3, 4) for UHV gauges and $u_{res}(p_G)/P_T$, which are corresponds to the standard deviation of the mean of the average value $\overline{p_x}$ obtained throughout the cycle. $u_A(a_{ijm})/a_{ijm}$ and $u_A(K_i)/K_i$ are calculated from data in Table 8 and Table 10, respectively, and shown without distinguishing where the data was obtained. $u_{res}(p_G)/P_T$ is calculated by the eq. (A10).

References

[1] Olson D. A., Abbott P. J., Jousten K., Redgrave F. J., Mohan P., Hong S. S., Metrologia, 2010, **47**, Tech. Suppl. 07004.

[2] Li D. and Jousten K., J. Vac. Sci. Technol. A, 2003, **21**(4), 937-946.

[3] Yoshida H., Arai K., Akimichi H., Hirata M., Vacuum, 2010, **84**, 705–708.

[4] Yoshida H., Hirata M., Akimichi H., Vacuum, 2011, **86**, 226-231.

[5] Takahashi N., Yuyama J., Tsuzi H., Arakawa I. J. Vac. Soc. Jpn., 2008, **51**, 377–381 [in Japanese].

[6] Hirata M., Sinku, 1994, **37**, 224–227 [in Japanese].

[7] Jousten K., Vacuum, 1998, **49**, 81-87.

[8] Abbott P. J., Looney J. P., Mohan P., Vacuum, 2005, **77**, 217–222.

[9] Wood S. D., Tilford C. R., J Vac Sci Technol. A, 1985, **3**, 542–545.

[10] Filippelli A. R. and Abbott P. J., J. Vac. Sci. Technol. A, 1995, **13**, 2582.

[11] Fedchak, J. A., Defibaugh D. R., J. Vac. Sci. Technol. A, 2012, **30**(6), 061601-1

[12] Messer G., Jitschin W., Rubet L., Calcatelli A., Redgrave R. J., Keprt A., Fei Wei-nan, Sharma J. K. N., Dittmann S., Ono M., Metrologia, 1989, **26**, 183-195.

[13] Sharma J. K. N., Mohan P., Jitschin W., Röhl P., J. Vac. Sci. Technol. A, 1989, **7**(4), 2788-2793.

[14] Hirata M., Bergoglio M., Calcatelli A., Rumiano G., Metrologia, 1997, **34**, 421-422.

[15] Jousten K., Filippelli A. R., Tilford C. R., Redgrave F. J., J. Vac. Sci. Tech. A, 1997, **15**, 2395.

[16] Jousten K., Bergoglio M., Calcatelli A., Durocher J., Greenwood J., Kangi R., Legras J., Matilla C., Setina J., Metrologia, 2005, **42**, 07001.

[17] Jousten K., Romero L. A. S., Guzman J. C. T., Metrologia, 2005, **42**, 07002.

[18] Yoshida H., Arai K., Akimichi H., Hong S. S., Song H. W., Metrologia, 2011, **48**, 7013 – 7076

[19] Medina N., Metrologia, 2011, **48**, 07014.

[20] Fedchak J. A., Bock T., Jousten K., Metrologia, 2014, **51**, 07005.

[21] Wuethrich C., Arai K., Bergoglio M., Fedchak J. A., Jousten K., Hong S. S., Guzman J. T., to be published.

[22] Fedchak J. A., Arai K., Jousten K., Setina J., Yoshida H., Measurement, 2015, **66**, 176-183.

[23] Jousten K., J. Vac. Sci. Technol. A, 2003, **21**(1), 318-324.

[24] Arai K., Yoshida H., Shiro M., Akimichi H., Hirata M., Abstracts of the 4th Vacuum and Surface Sciences Conference of Asia and Australia (VASSCAA-4), Matsue

(2008) p. 359.

[25] Yoshida H., Shiro M., Arai K., Akimichi H., Hirata, M., Vacuum, 2010, **84**, 277.

[26] Arai K., Akimichi H., Hirata M., J. Vac. Soc. Jpn., 2010, **53**, 614 [in Japanese].

[27] Jousten K., Menzer H., Wandrey D., Niepraschk R., Metrologia, 1999, **36**, 493.

[28] Jousten K., Menzer H., Niepraschk R., Metrologia, 2002, **39**, 519.

[29] Tanaka H., Kenzai Shiken Jouhou, 2003, **12**, 6-12 [in Japanese].

[30] Tanaka H., Bunseki, 2010, **4**, 168-174 [in Japanese].